nature physics

LETTERS

PUBLISHED ONLINE: 12 OCTOBER 2015 | DOI: 10.1038/NPHYS3508

Coherent long-range magnetic bound states in a superconductor

Gerbold C. Ménard[1], Sébastien Guissart[2], Christophe Brun[1], Stéphane Pons[1,3], Vasily S. Stolyarov[1,4], François Debontridder[1], Matthieu V. Leclerc[1], Etienne Janod[5], Laurent Cario[5], Dimitri Roditchev[1,3], Pascal Simon[2]* and Tristan Cren[1]*

The quantum coupling of fully different degrees of freedom is a challenging path towards new functionalities for quantum electronics[1–3]. Here we show that the localized classical spin of a magnetic atom immersed in a superconductor with a two-dimensional electronic band structure gives rise to a long-range coherent magnetic quantum state. We experimentally evidence coherent bound states with spatially oscillating particle–hole asymmetry extending tens of nanometres from individual iron atoms embedded in a 2H-$NbSe_2$ crystal. We theoretically elucidate how reduced dimensionality enhances the spatial extent of these bound states and describe their energy and spatial structure. These spatially extended magnetic states could be used as building blocks for coupling coherently distant magnetic atoms in new topological superconducting phases[4–11].

Coupling different degrees of freedom of both quantum and classical objects yields new quantum functionalities not available in each system taken separately. In this regard, new hybrid quantum systems have been recently designed, such as individual atoms and optical cavities coupled through photon exchange[1], or a single quantum dot coupled to a mechanical oscillator through strain[2].

Recently, a new type of electronic excitation, being its own antiparticle, was predicted to appear at the edges of a hybrid system consisting of a chain of magnetic atoms coupled to a superconductor[7]. These so-called Majorana end-states have allegedly been observed in the case of chains of iron atoms on Pb (110) (ref. 3); however, their spatial extent is restricted to a few atomic distances, making it difficult to handle them for braiding.

An alternative proposal for manipulating Majorana quasiparticles consists in engineering a one-dimensional topological superconductor in a chain of magnetic atoms with a spiral magnetic order on the surface of a superconductor[4–11]. Individual local magnetic moments act destructively on Cooper pairs, leading to discrete spin-polarized states inside the superconducting energy gap, as predicted by Yu, Shiba and Rusinov[12–14] (YSR). Rusinov suggested that around magnetic atoms the decaying YSR wavefunction should have a spatially oscillating structure[14–16]. The emergence of topological superconductivity depends on YSR-states-mediated coupling inside the magnetic chain[10].

Although Nadj-Perge *et al.*[3] relied on a direct interaction between neighbouring atoms to generate short-ranged Majorana quasiparticles, in the latter case the characteristic length is that of the YSR bound states, which may extend up to the scale of the superconducting coherence length. Enhancing the spatial extent of the YSR bound states would facilitate the remote coupling of magnetic systems through a superconducting state, opening the route towards an easier manipulation of Majorana quasiparticles and the creation of new topological quantum devices.

Here we reveal that the dimensionality plays a critical role in the spatial decay of the YSR bound states. Calculations using Rusinov's approach[14] are presented in Fig. 1a–d. They show that a three-dimensional isotropic *s*-wave superconductor induces a marked decay of the YSR states out of the magnetic impurity. These calculations are in agreement with the atomically short spatial extent of the YSR states observed in all previous scanning tunnelling microscopy (STM) studies of single magnetic impurities in superconductors: Co, Cr, Mn, or Gd atoms deposited on Pb or Nb crystals[17,18] and manganese-phtalocyanine molecules deposited on Pb (ref. 19). By extending this theory to two dimensions (2D), we evidence in Fig. 1e–g that superconductors with two-dimensional electronic structure should host YSR bound states with spatial extents orders of magnitude larger. Hence, layered superconducting materials such as 2H–$NbSe_2$, known for their two-dimensional character, are good candidates for supporting these long-range quantum states[20].

In this work, we studied single crystals of 2H–$NbSe_2$ containing a few tens of ppm of magnetic impurities. The chemical analysis of the sample indicates that the main magnetic impurity present is Fe (see Methods). Atomically resolved topographic STM imaging of the surface (Fig. 2b) exhibits the characteristic charge density wave pattern. Individual impurities are visible as bright or dark spots. Whereas on topographic STM images the magnetic and non-magnetic impurities cannot be distinguished, the magnetic impurities are the only ones to present a characteristic spectroscopic signature inside the superconducting gap (see Methods).

The scanning tunnelling spectroscopy studies performed at 320 mK, well below the critical temperature of 7.2 K, reveal YSR bound states around the randomly dispersed magnetic iron impurities in 2H–$NbSe_2$ (see Methods). Remarkably, these states are characterized by a six-pointed star-shaped electronic signature extending as far as 10 nm from defects, as can be seen in Fig. 2d. This is more than ten times larger than the previously observed extension of YSR bound states[17–19] and is comparable to the in-plane coherence length of 2H–$NbSe_2$. This long-range pattern is due to the two-dimensional character of 2H–$NbSe_2$ (see Fig. 1), as opposed to the observed short range in three-dimensional materials such as Pb or Nb. This unusually long spatial effect may also be amplified by

[1]Institut des Nanosciences de Paris, Sorbonne Universités, UPMC Univ Paris 6 and CNRS-UMR 7588, F-75005 Paris, France. [2]Laboratoire de Physique des Solides, Université Paris-Sud, 91405 Orsay, France. [3]Laboratoire de physique et d'étude des matériaux, LPEM-UMR8213/CNRS-ESPCI ParisTech-UPMC, 10 rue Vauquelin, 75005 Paris, France. [4]Moscow Institute of Physics and Technology, 141700 Dolgoprudny, Russia. [5]Institut des Matériaux Jean Rouxel, CNRS Université de Nantes, UMR 6502, 2 rue de la Houssinière, BP32229, 44322 Nantes, France. *e-mail: pascal.simon@u-psud.fr; tristan.cren@upmc.fr

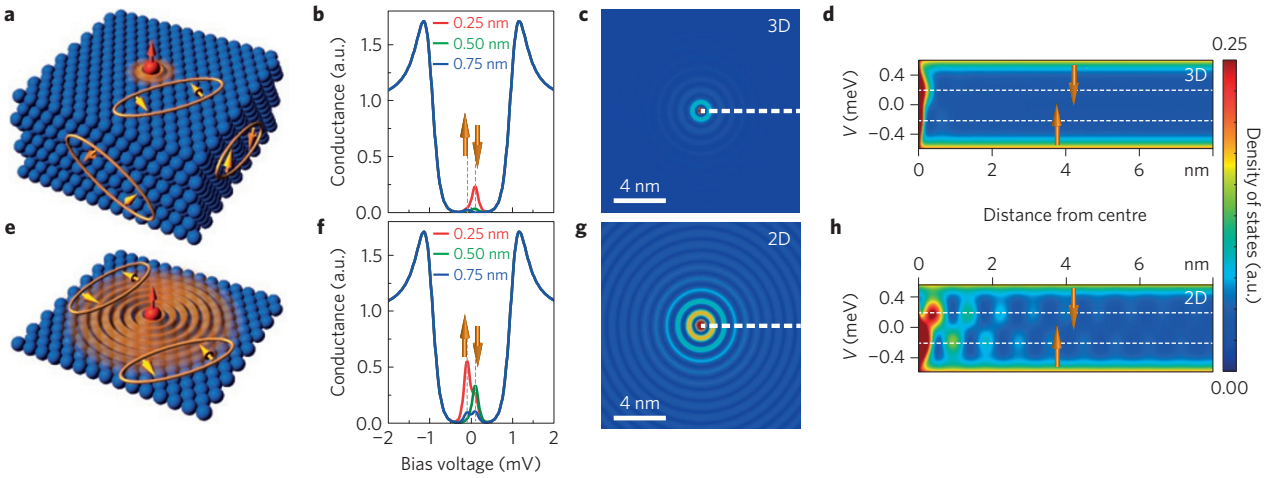

Figure 1 | Comparison between 3D and 2D for the spatial extent of Yu–Shiba–Rusinov states. a–h, Calculated behaviour of a Yu–Shiba–Rusinov bound state in an isotropic *s*-wave superconductor with three-dimensional (**a**–**d**) and two-dimensional (**e**–**h**) electronic band structure. **a**,**e**, Schematic views of the interaction of Cooper pairs with a classical magnetic impurity. **b**,**f**, Calculated scanning tunnelling spectra at various distances from the impurity, showing the fully polarized YSR states inside the superconducting gap. **c**,**g**, Simulated conductance maps around the impurity, showing the spatial extent of one peak of the YSR state presented in **b** and **f**, respectively. **d**,**h**, Simulated conductance between −0.6 and 0.6 mV along the dotted line out of the impurity in **c** and **g**, respectively.

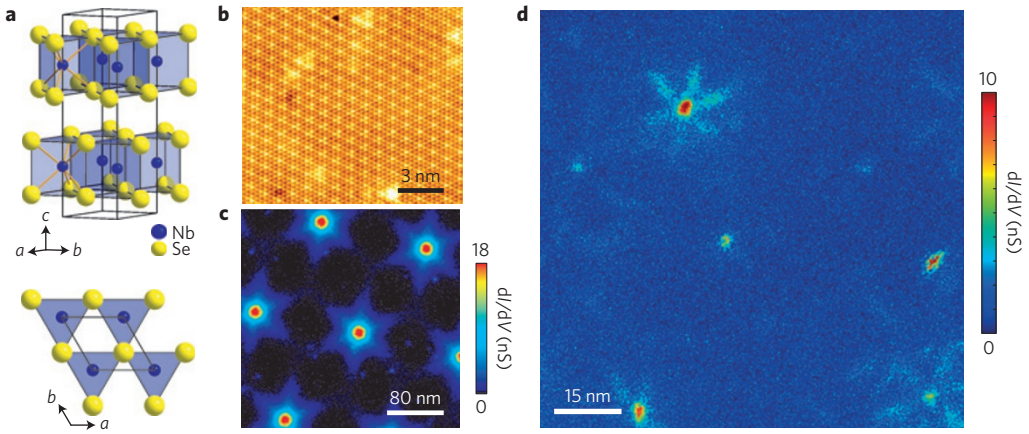

Figure 2 | Structural and superconducting properties of 2H-$NbSe_2$. a, Atomic structure of a 2H-$NbSe_2$ crystal. **b**, 19×17 nm^2 topographic image of a 2H-$NbSe_2$ sample with the atomic lattice modulated by a charge density wave. The image is taken at $V = -200$ meV and $I = 80$ pA. **c**, Abrikosov lattice in 2H-$NbSe_2$, showing the star-shaped structure of vortices in a magnetic field of 0.1 T. **d**, Conductance map taken at $V = -0.05$ meV, integrated over ± 0.02 meV, showing a few star-shaped structures created by localized magnetic impurities at zero magnetic field. Measurements were performed at 320 mK.

the fact that the Fe impurities are embedded in the atomic lattice. Therefore, they may experience a stronger electronic coupling to the superconducting condensate than the adsorbed impurities used in previous experiments.

The arms of the star-shaped pattern of the YSR states are turned by 30° with respect to the crystallographic axes of 2H–$NbSe_2$ (Fig. 2a), which corresponds to the reciprocal lattice vectors ($\mathbf{a}^*$ and $\mathbf{b}^*$). This orientation is also the same as that of the star-shaped vortices observed in 2H–$NbSe_2$ (Fig. 2c). In addition to the dominant type of impurity shown on Figs 2d and 3a attributed to Fe atoms, we also observe impurities of Cr and Mn giving star-shaped structures with the same orientation, but with a thicker pattern and slightly different YSR energies (see Supplementary Information 2). Therefore, this six-fold symmetry is likely to arise from a common origin, and in both cases reflects the anisotropy of the Fermi surface[20], as supported by our simulations.

The tunnelling spectra acquired over a chosen Fe impurity (see spectroscopic map in Fig. 3a) show a YSR bound state which takes the form of two peaks at positive and negative energies ($E_{\mathrm{Shiba}} \simeq \pm 0.2\Delta$) inside the superconducting gap of 2H–$NbSe_2$ (red curve in Fig. 3b). Apart from the YSR state, the characteristic superconducting spectrum is perfectly preserved. The YSR peak at negative bias is much stronger than the peak at positive bias, highlighting a strong particle–hole asymmetry near the magnetic atom, as presented in Fig. 1h. The presence of a single pair of YSR peaks in the gap indicates that the *s*-wave diffusion channel (angular momentum $l = 0$) dominates. As the allowed values for the angular momentum depend on the shape and extent of the diffusion potential, observing only the $l = 0$ diffusion channel suggests that the iron impurities may be considered as point defects. Similarly, in Gd/Nb, Mn/Nb (ref. 17) or Mn-phtalocyanine on Pb (ref. 19), the $l = 0$ diffusion channel was the only one to be activated. In contrast, for Mn/Pb, YSR states for $l = 0$ and $l = 1$ were observed and $l = 2$ states were found for Cr/Pb(111) (ref. 18). However, in all these works, the spectroscopic signatures associated with the impurities completely vanished a few Å from their centre. In this context our

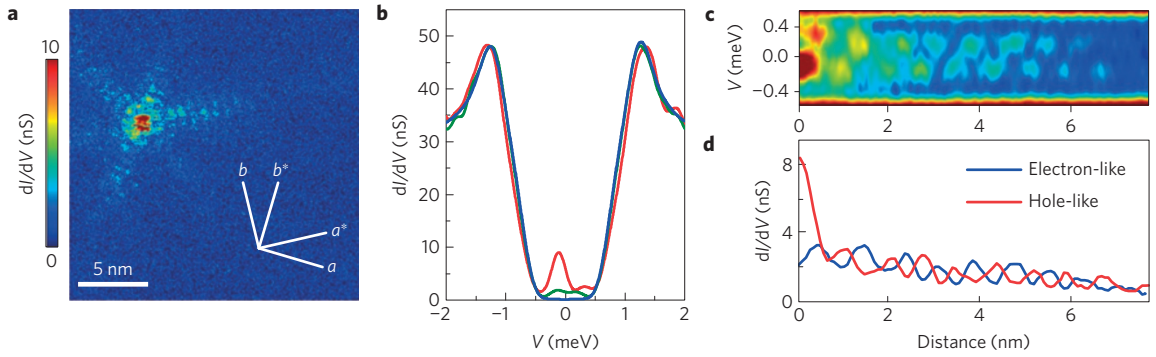

Figure 3 | Spectral and spatial properties of an extended Yu–Shiba–Rusinov bound state in 2H–$NbSe_2$. **a**, Experimental conductance map taken at −0.13 meV. The *a* and *b* lines indicate the crystallographic axes of 2H–$NbSe_2$, whereas the *a** and *b** lines indicate the directions in the reciprocal space. **b**, Characteristic experimental spectra taken on top of the impurity (red), on the right branch, 4 nm from the centre of the impurity (green), and far from the impurity (blue). **c**, Spatial and energy evolution of the experimental tunnelling conductance spectra, $dI/dV(x, V)$ along one branch of the star. The left side of the figure corresponds to the centre of the star and the right side to the top-right corner of the scanning area. The colour conductance scale is the same as that used in **a**. **d**, Conductance profiles of the electron- and hole-like YSR states as a function of the distance to the impurity along the same line as for **c**.

measurements show that the local nature of the interaction does not prevent the existence of a long-range effect on the density of states.

To recover the symmetry of the observed YSR bound state one needs to take into account the band structure of the material. The hexagonal symmetry observed experimentally in Figs 2d and 3a is reproduced well in the framework of the Bogoliubov–de Gennes formalism[21]. This is done by numerically solving the Schrödinger equation with an almost exact tight-binding description of the band structure of 2H–$NbSe_2$ (see Supplementary Information 3). As we observe only $l = 0$ states we assume a strictly on-site interaction while treating the magnetic impurity classically—that is, assuming a large spin number S (see Supplementary Information 1). The interaction potential contains both a magnetic and non-magnetic part and reads as

$$H_{\mathrm{Imp}} = -\frac{JS}{2}(c^{\dagger}_{0\uparrow}c_{0\uparrow} - c^{\dagger}_{0\downarrow}c_{0\downarrow}) + K(c^{\dagger}_{0\uparrow}c_{0\uparrow} + c^{\dagger}_{0\downarrow}c_{0\downarrow})$$

where the c_0 and $c^{\dagger}_0$ operators are respectively the annihilation and creation operators for electrons with spin σ on the magnetic atom site. The first term corresponds to a Zeeman splitting between spin-up and spin-down electrons for a coupling strength $J/2$ between the superconducting electrons and the individual atom. The second term is a non-magnetic diffusion potential of amplitude K. Using this approach, we calculate the local density of states (LDOS) for both the electron-like and hole-like YSR state. Because our experimental data are obtained in the large tip–sample distance regime, the measured current is carried by single-electron tunnelling rather than by Andreev processes[22]. Therefore, we can directly compare the calculated LDOS with the experimental data and we recover the typical star-shaped structure, as presented on Fig. 4, aligned along the reciprocal lattice vectors.

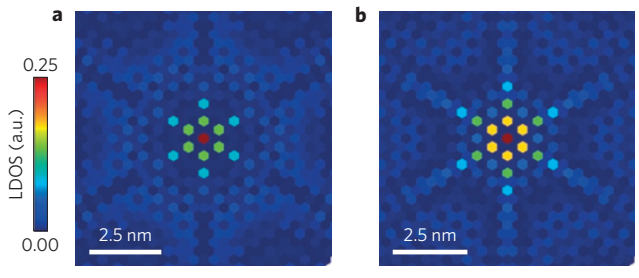

Figure 4 | Tight-binding calculation of the spatial structure of Yu–Shiba–Rusinov states. Local density of state (LDOS) computed with $JS/2 = 120$ meV and $K = -180$ meV. **a**, LDOS for electron-like YSR states with energy $E_{\mathrm{Shiba}} = 0.59\Delta$. **b**, LDOS for hole-like YSR states with energy $E_{\mathrm{Shiba}} = -0.59\Delta$.

We now focus on the details of the star presented on the experimental spectroscopic map, taken at the energy of the strongest YSR peak −0.13 mV (see Fig. 3a). The high tunnelling conductance in the centre of the star (red colour) corresponds to a very strong peak in the tunnelling spectra (red curve on Fig. 3b) localized on the impurity[22]. On the surrounding tail the amplitude of YSR peaks decreases, as shown by the green conductance curve of Fig. 3b acquired at 4 nm away from the impurity. This decrease is oscillatory, resulting in interference fringes with a periodicity of 0.8 nm, clearly visible on the conductance map. The evolution of the conductance spectra along one arm of the star is shown in Fig. 3c. The interference fringes in the conductance for the electron and hole excitations are in an almost perfect spatial antiphase. It seems that a few nanometres away from the impurities the tail of the YSR states exhibits a similar amplitude for the electron-like and hole-like excitations (see Fig. 3c,d)—that is, the particle–hole symmetry is progressively restored away from the defect. Our analysis shows that the oscillations are due to the scattering of electrons by the impurity at the saddle points between the pocket around Γ and the pockets around the K points of the Fermi surface of 2H–$NbSe_2$.

The observed oscillations being of the order of the Fermi wavelength, they cannot be captured by a discrete tight-binding model. Following Rusinov[14] and taking the continuum limit description of the equation giving access to the YSR states, we extract the asymptotic behaviour of the wavefunction far from the magnetic impurity (see Supplementary Information 5). We qualitatively reproduce the two characteristic length scales of the experimentally observed interference pattern. Assuming an isotropic energy band, the YSR energy can be parametrized as $E = \Delta\cos(\delta^{+} - \delta^{-})$ (ref. 14), with $\tan\delta^{\pm} = K\nu_0 \pm JS/2\nu_0$ where ν_0 is the density of states at the Fermi energy. In 2D the YSR wavefunction can be shown to behave at large distances from the impurity as (see Supplementary Information 5):

$$\psi_{\pm}(r) = \frac{1}{\sqrt{N\pi k_{\mathrm{F}} r}}\sin\left(k_{\mathrm{F}}r - \frac{\pi}{4} + \delta^{\pm}\right)\mathrm{e}^{-\Delta\sin(\delta^{+}-\delta^{-})r/\hbar v_{\mathrm{F}}}$$

where ψ_{+} and ψ_{-} denote respectively the electron and hole components of the YSR wavefunction ψ, N is a normalization factor, k_{F} is the Fermi wavevector and v_{F} the Fermi velocity. This behaviour is presented in Fig. 1. H is in excellent agreement with

the experimental Fig. 3c,d. This result highlights the dimensionality dependence, as the decay of the local density of states goes as $1/r$ in 2D and $1/r^2$ in 3D (see Supplementary Information 6). Furthermore, for deep YSR states, which correspond to a dephasing $\delta^+ - \delta^- \longrightarrow \pm\pi/2$, the electron and hole YSR density of states are indeed in antiphase far enough from the impurity. In our approach each component of the YSR states is fully polarized both in spin and charge. The analytical equation links the long-distance decay of the YSR state to the superconducting coherence length and the oscillatory behaviour to the Fermi wavelength.

In conclusion, by coupling a classical spin to a superconductor with a two-dimensional electronic structure we were able to unveil a long-range coherent magnetic quantum state with a spatially oscillating electron–hole asymmetry. As this effect is related to the dimensionality it should manifest in a wide variety of superconductors, such as lamellar materials or recently discovered superconducting monolayers of Pb/Si(111), In/Si(111) (refs 23,24) and FeSe/$SrTiO_3$ (ref. 25). The interaction between long-range YSR states has now to be explored. Subsequently, it could be used to produce new topological phases in hybrid systems. Arrays of magnetic atoms and molecules coupled through a superconducting medium are indeed expected to present a large variety of topological orders[26]. For instance, a chain of magnetic atoms coupled through the spatially extended YSR bound states with a helical spin order could lead to a topological triplet superconductivity with Majorana quasiparticles at its extremities[4–11].

Methods

Methods and any associated references are available in the online version of the paper.

Received 3 June 2015; accepted 11 September 2015; published online 12 October 2015

References

1. Thompson, J. D. *et al.* Coupling a single trapped atom to a nanoscale optical cavity. *Science* **340,** 1202–1205 (2013).
2. Yeo, I. *et al.* Strain-mediated coupling in a quantum dot-mechanical oscillator hybrid system. *Nature Nanotech.* **9,** 106–110 (2014).
3. Nadj-Perge, S. *et al.* Observation of Majorana fermions in ferromagnetic atomic chains on a superconductor. *Science* **346,** 602–607 (2014).
4. Nadj-Perge, S., Drozdov, I. K., Bernevig, B. A. & Yazdani, A. Proposal for realizing Majorana fermions in chains of magnetic atoms on a superconductor. *Phys. Rev. B* **88,** 020407(R) (2013).
5. Choy, T.-P., Edge, J. M., Akhmerov, A. R. & Beenakker, C. W. J. Majorana fermions emerging from magnetic nanoparticles on a superconductor without spin–orbit coupling. *Phys. Rev. B* **84,** 195442 (2011).
6. Nakosai, S., Tanaka, Y. & Nagaosa, N. Two-dimensional *p*-wave superconducting states with magnetic moments on a conventional *s*-wave superconductor. *Phys. Rev. B* **88,** 180503(R) (2013).
7. Braunecker, B. & Simon, P. Interplay between classical magnetic moments and superconductivity in quantum one-dimensional conductors: Toward a self-sustained topological Majorana phase. *Phys. Rev. Lett.* **111,** 147202 (2013).
8. Klinovaja, J., Stano, P., Yazdani, A. & Loss, D. Topological superconductivity and Majorana fermions in RKKY systems. *Phys. Rev. Lett.* **111,** 186805 (2013).
9. Vazifeh, M. M. & Franz, M. Self-organized topological state with Majorana fermions. *Phys. Rev. Lett.* **111,** 206802 (2013).
10. Pientka, F., Glazman, L. I. & von Oppen, F. Topological superconducting phase in helical Shiba chains. *Phys. Rev. B* **88,** 155420 (2013).
11. Kim, Y., Cheng, M., Bauer, B., Lutchyn, R. M. & Das Sarma, S. Helical order in one-dimensional magnetic atom chains and possible emergence of Majorana bound states. *Phys. Rev. B* **90,** 060401(R) (2014).
12. Yu, L. Bound state in superconductors with paramagnetic impurities. *Acta Phys. Sin.* **21,** 75–91 (1965).
13. Shiba, H. Classical spins in superconductors. *Prog. Theor. Phys.* **40,** 435–451 (1968).
14. Rusinov, A. I. Superconductivity near a paramagnetic impurity. *JETP Lett.* **9,** 85–87 (1969).
15. Bauriedl, W., Ziemann, P. & Buckel, W. Electron-tunneling observation of impurity bands in superconducting manganese-implanted lead. *Phys. Rev. Lett.* **47,** 1163–1165 (1981).
16. Balatsky, A. V., Vekhter, I. & Zhu, J.-X. Impurity-induced states in conventional and unconventional superconductors. *Rev. Mod. Phys.* **78,** 373–433 (2006).
17. Yazdani, A., Jones, B. A., Lutz, C. P., Crommie, M. F. & Eigler, D. M. Probing the local effects of magnetic impurities on superconductivity. *Science* **275,** 1767–1770 (1997).
18. Ji, S.-H. *et al.* High-resolution scanning tunneling spectroscopy of magnetic impurity induced bound states in the superconducting gap of Pb thin films. *Phys. Rev. Lett.* **100,** 226801 (2008).
19. Franke, K. J., Schulze, G. & Pascual, J. I. Competition of superconducting phenomena and Kondo screening at the nanoscale. *Science* **332,** 940–944 (2011).
20. Rossnagel, K. *et al.* Fermi surface of 2H–$NbSe_2$ and its implications on the charge-density-wave mechanism. *Phys. Rev. B* **64,** 235119 (2001).
21. Flatté, M. E. & Reynolds, D. E. Local spectrum of a superconductor as a probe of interactions between magnetic impurities. *Phys. Rev. B* **61,** 14810–14814 (2000).
22. Ruby, M. *et al.* Tunneling processes into localized subgap states in superconductors. *Phys. Rev Lett.* **115,** 087001 (2015).
23. Zhang, T. *et al.* Superconductivity in one-atomic-layer metal films grown on Si(111). *Nature Phys.* **6,** 104–108 (2010).
24. Brun, C. *et al.* Remarkable effects of disorder on superconductivity of single atomic layers of lead on silicon. *Nature Phys.* **10,** 444–450 (2014).
25. Wang, Q. Y. *et al.* Interface-induced high-temperature superconductivity in single unit-cell FeSe films on $SrTiO_3$. *Chin. Phys. Lett.* **29,** 037402 (2012).
26. Röntynen, J. & Ojanen, T. Topological superconductivity and high Chern numbers in 2D ferromagnetic Shiba lattices. *Phys. Rev. Lett.* **114,** 236803 (2015).

Acknowledgements

This work was supported by the French Agence Nationale de la Recherche through the contracts ANR Electrovortex and ANR Mistral. G.C.M. acknowledges funding from the CFM foundation providing his PhD grant. V.S.S. thanks L. R. Tagirov for his assistance. The authors thank E. Canadell, K. Behnia and V. Vinokur for stimulating discussions.

Author contributions

D.R., T.C. and F.D. designed the experiments. G.C.M., C.B., T.C., D.R., V.S.S., M.V.L. and S.P. carried out the experiments. G.C.M. and T.C. processed and analysed the data. S.G. and P.S. performed the theoretical modelling. L.C. and E.J. grew the samples and performed the chemical analysis. All authors discussed the results and took part in the correction of the manuscript.

Additional information

Supplementary information is available in the online version of the paper. Reprints and permissions information is available online at www.nature.com/reprints. Correspondence and requests for materials should be addressed to P.S. or T.C.

Competing financial interests

The authors declare no competing financial interests.

Methods

2H–$NbSe_2$ crystals were synthesized using an iodine transport method. Stoichiometric amounts of the elements (Nb 99.8% Alfa Aesar, Se 99.99% Aldrich) were sealed under vacuum in a silica tube with a small amount of iodine (4 mg cm^{-3}, 99.9985% Puratronic). The tube was then heated up for a period of 170 h in a gradient furnace. The mixture was located in the high-temperature zone of the furnace at 700 °C, while the cold-temperature end of the tube was held at around 660 °C (gradient 3 °C cm^{-1}). This synthesis yielded large shiny black layered crystals (400 μm in size) along with some black powder. X-ray diffraction patterns of the powder revealed that it is composed of a majority of the 2H–$NbSe_2$ phase (90%). Five single crystals were then tested for crystallographic quality using a four-circle FR 590 Nonius CAD-4F κ-CCD diffractometer at 300 K. All of them revealed a hexagonal cell with parameters $a = b \simeq 3.44$ Å and $c \simeq 12.56$ Å, in very good agreement with parameters reported for the 2H–$NbSe_2$ phase[27]. Finally, the composition of several crystals was tested by energy dispersive X-ray spectroscopy using an electronic microscope (JEOL JSM 5800LV). A ratio Nb/Se close to 1:2 was measured, in agreement with the chemical formula. No impurity traces could be detected using this technique, as the threshold of detection is larger than 1,000 ppm. However, the certificate of analysis delivered by the supplier (Alfa Aesar) for the niobium powder used as precursor (lot number K08Q025) revealed as the main magnetic impurities 175 ppm of Fe, 54 ppm of Cr and 22 ppm of Mn. This synthesis, therefore, yielded 2H–$NbSe_2$ crystals unintentionally doped by a few tens of ppm of magnetic species.

The scanning tunnelling spectroscopy measurements were performed *in situ* with a in-house-built apparatus at a base temperature of 320 mK and in an ultrahigh vacuum with $P < 1.10^{-10}$ mbar. The 2H–$NbSe_2$ sample was cleaved *in situ*. Mechanically sharpened Pt/Ir tips were used. A bias voltage was applied to the sample with respect to the tip. Typical set-point parameters for spectroscopy are 120 pA at $V = -5$ mV. The electron temperature was estimated to be 360 mK. The tunnelling conductance curves dI/dV were numerically differentiated from raw $I(V)$ experimental data. Each conductance map is extracted from a set of data consisting of spectroscopic $I(V)$ curves measured at each point of a 256×256 grid, acquired simultaneously with the topographic image. Each $I(V)$ curve contains 1,200 energy points.

References

27. Selte, K. & Kjekshus, A. On the structural properties of the $Nb_{1+x}Se_2$ phase. *Acta Chem. Scand.* **18,** 697–706 (1964).